(In Press) Engr. Fracture Mechanics Jl.

FBR 8503

COLLEGE OF ENGINEERING

VPI-E-74-13

A STUDY OF NEAR AND FAR FIELD EFFECTS IN PHOTOELASTIC STRESS INTENSITY DETERMINATION

by

M. A. Schroedl* and C. W. Smith**

Department of Engineering Science & Mechanics

July 1974

VIRGINIA POLYTECHNIC INSTITUTE AND STATE UNIVERSITY

BLACKSBURG, VIRGINIA

College of Engineering
Virginia Polytechnic Institute & State University
Blacksburg, Virginia 24061

VPI-E-74-13

A STUDY OF NEAR AND FAR FIELD EFFECTS IN PHOTOELASTIC STRESS INTENSITY DETERMINATION

by

M. A. Schroedl* and C. W. Smith**

Department of Engineering Science & Mechanics

July 1974

Reporting Period: Winter and Spring 1974

Prepared for:

Department of Defense, U.S. Army
Contract No. DAA-F07-69-C-0444 with
Watervliet, Arsenal
Watervliet, New York

*Research Engineer - Firestone Central Research Laboratory, Akron, Ohio

**Professor

ABSTRACT

A technique known as the Taylor Series Correction Method (TSCM) for extracting the stress intensity factor from photoelastic data is reviewed. The need for "artificial" flaws is identified and an approach due to Savin is used to evaluate the near field effects of various practical flaw shapes upon the apparent stress intensity factor. Using the Sneddon-Srivastav solution for a line crack in a finite width plate, the constriction of the singular zone is demonstrated as the crack tip approaches the free edge. Results indicate that care must be taken in applying TSCM to obtain photoelastic data at appropriate distances from the crack tip.

LIST OF SYMBOLS

r, θ	Polar coordinates as defined in Figure 1.
x, y	Cartesian coordinates as defined in Figure 1.
$\bar{x}, \bar{y}$	Nondimensional coordinates x/w, y/w as shown in Figure 9.
a	Crack length or depth (for surface flaws).
b	Width of symmetrical notch at center (Figure 4).
t	Specimen thickness.
w	Width of finite width strip.
α	Notch angle (Figure 4) or elliptical flaw angle.
z	Complex variable $x + iy$ (Figure A-1).
$\bar{z}$	Complex variable $\bar{x} + i\bar{y}$ (Figure 9).
ρ	Radius of curvature of notch at tip.
n	Fringe order.
N	Number of data points.
f	Material fringe value.
τ_{max}	Maximum shear stress in plane perpendicular to the crack border.
$\bar{\sigma}$	Remote tensile stress.
σ_0	Regular or non-singular stress parallel to the crack at the crack tip.
δ	σ_0/σ

K_I, SIF	Mode I stress intensity factor.
K_{AP}	Apparent stress intensity factor $\tau_{max}\sqrt{8\pi r}$ along $\theta = \frac{\pi}{2}$ in Figure 1.
σ_x, σ_y, τ_{xy}	Stress components in a plane perpendicular to the crack border.
$\bar{\sigma}_x$, $\bar{\sigma}_y$, $\bar{\tau}_{xy}$	Stress components nondimensionalized with respect to the remote tension $\bar{\sigma}$.
J_0, J_1	Bessel functions of the first kind.
I_0, I_1	Modified Bessel functions of the first kind.
G(t)	Solution of Fredholm integral equation (6).
ζ	Complex variable $\xi + i\eta$ defined in Figure A-1.
$\omega(\zeta)$	Mapping function which maps ζ into z in Figure A-1.
ϕ_1, ϕ_2	Mapping angles defined in Figure A-1.
ϕ, ψ	Muskhelishvili potentials.
A_i	Least squares coefficients for G(t) in equation (11).
B_i	Coefficients in Taylor Series Correction Method of equation (5).
TSCM	Taylor Series Correction Method.
$\hat{\sigma}$	Dummy variable.

TABLE OF CONTENTS

FIGURES

INTRODUCTION

Although the use of photoelasticity for determining stress intensity factors was suggested by Irwin [1] as early as 1952, extensive employment of the method has been slow to develop. There are a number of reasons for this. Results of Fessler and Mansell [2] and Marloff et al [3] revealed the need for highly accurate measurements, and their studies were reinforced by those of Kobayashi [4]-[6] and his associates in their work with propagating cracks. Liebowitz, Vanderveldt and Sanford [7] also noted certain near field effects which affected stress intensity factor (SIF) determination. In order to obtain valid data for SIF determination one must take the data in a zone dominated by the singular stresses. This zone is bounded on the outside by a zone strongly affected by the remote boundaries and loads, and on the inside by a zone dominated by very local effects. These very local effects for a stress freezing photoelastic material consist of two types:

1) Non-linear effects which accrue from finite rotations and deformations near initially sharp crack tips.

2) Notch geometry effects when the crack is simulated with a notch, or when the crack opens a substantial amount, producing blunting. Beginning in 1969, the senior author and his associates carried out a series of stress freezing photoelastic investigations [8]-[19]. These studies revealed that, in a number of three dimensional problems [13]-[15] the zone dominated by the singular stresses was severely constricted and that it was necessary to use data outside the singular zone for SIF determination. In order to account for remote effects included in this way, a technique employing a Taylor series expansion of the maximum in-plane shear stress to account for the regular part of the stress field was employed. The method is referred to

as the Taylor Series Correction Method (TSCM). Details of the method have been described in [14] and [17] and its applicability to three dimensional problems was recently discussed in [20]. (This method will be featured in a chapter in the second volume of the SESA Monograph on Experimental Fracture Mechanics). Although the use of TSCM has extended the applicability of photoelastic SIF determination to three dimensional problems not previously solved, practical difficulties remain in fabricating appropriate crack geometries, producing effects upon the inner zone previously mentioned. Moreover, analytical verification of the constriction of the singular zone due to free boundaries or three dimensional effects has not been demonstrated. In a very recent analytical study [21] McGowan and Smith have shown that the non-linear effects in the inner zone are much too near the crack or notch tip to be picked up in the photoelastic data. However, in problems where a specific crack shape is desired, an artificial crack may be sawed in, producing a relatively large root radius, or the photoelastic material in the rubbery range may stretch enough locally near the crack tip under even small loads to produce stress field disturbances which may extend into the photoelastic data zone. The present study is concerned with a quantitative analytical assessment of effects of this type, and also with a two dimensional analytical study of the influence of free boundaries upon the singular zone.

BASIC THEORY

The Irwin Equations [1] for the elastic stress field near the tip of a plane crack are:

$$\sigma_x = \frac{K_I}{(2\pi r)^{1/2}} \cos\frac{\theta}{2}\left\{1 - \sin\frac{\theta}{2}\sin\frac{3\theta}{2}\right\} - \sigma_0$$

$$\sigma_y = \frac{K_I}{(2\pi r)^{1/2}} \cos\frac{\theta}{2}\{1 + \sin\frac{\theta}{2}\sin\frac{3\theta}{2}\} \quad (1)$$

$$\tau_{xy} = \frac{K_I}{(2\pi r)^{1/2}} \sin\frac{\theta}{2}\cos\frac{\theta}{2}\cos\frac{3\theta}{2}$$

with the notation given in Figure 1. This discussion will be confined to plane problems so that complete solutions can be employed in all mathematical models. Application of the method to three dimensional problems is described elsewhere, [14], [19], [20]. The quantity measured photoelastically is the fringe order which is proportional to the maximum in-plane shearing stress. The local value of this latter quantity may be computed by substituting Equations (1) into:

$$\tau_{max} = \frac{1}{2}\sqrt{(\sigma_x - \sigma_y)^2 + 4\tau_{xy}^2} \quad (2)$$

Then evaluating τ_{max} along the convenient direction $\theta = \pi/2$ and combining this result with the stress optic law

$$\tau_{max} = \frac{nf}{2t} \quad (3)$$

one can obtain:

$$K_I = (\pi r)^{1/2}\left[\{2\left(\frac{nf}{t}\right)^2 - \sigma_0^2\}^{1/2} - \sigma_0\right] \quad (4)$$

Equations (1) constitute a two parameter (K_I,σ_0) set of field equations and are valid, according to Irwin in the singular zone.

When one uses data outside this zone, the following equation may be used:

$$\tau_{max} = \frac{K_I}{(8\pi r)^{1/2}} + \sum_{N=0}^{M} B_N r^N \quad (5)$$

instead of Equation (4) where the first term arises from the singular stresses and the Taylor Series accounts for the regular part of the stress field including σ_0. Use of Equation (5) is made in the TSCM and the number

of degrees of freedom of the system can be greater than two (i.e. K_I, B_0, B_1, B_2, . . . B_n) but normally does not exceed five or six.

Although one normally would expect to plot stress (i.e. τ_{max}) versus distance from the crack tip, the authors have found this type of plot to be relatively insensitive to changes in the stress intensity factor. Instead, an apparent stress intensity factor is defined as:

$$K_{AP} = (8\pi r)^{1/2} \tau_{max} \tag{6}$$

and a normalized value of this quantity is plotted against $(r/a)^{1/2}$. Extrapolation of this curve to r/a = 0 yields the experimental SIF.

NOTCH EFFECTS

Figure 2 is a microphoto of a natural flaw under a field of remote tension perpendicular to the crack plane showing how a "hairline" crack opens under tension into a geometry approximating a narrow ellipse. This blunts the crack tip into a root radius of about 5×10^{-3} mm. An assessment of the influence of this blunting was made by the authors in an earlier paper [12] by computing the apparent SIF from the Inglis-Kolosoff linearly elastic solution for an elliptical hole in an infinite plate under tension and normalizing it with respect to the SIF for a line crack in an infinite plate. The results are shown in Figure 3 and reveal a blunting effect which is negligible only if data are taken at least five to ten root radii from the crack tip.

Artificial notches may be made in a variety of geometries. A series of those found convenient by the authors are pictured in Figure 4 together with the elliptical notch just discussed. Approximate mapping functions have been provided by Savin [22] which lead to the determination of the

Muskhelishvili complex potentials [23] from which complete solutions to these geometries may be obtained. Such procedures are detailed in Appendix A for the geometries (other than elliptical) of Figure 4.

The solution for a rectangular notch was obtained as a special case of the general mapping solution presented in Appendix A. The solution is exact for the region of the z plane corresponding to the unit circle in the ζ plane. This region is not, however, an exact rectangle but has curvilinear sides and corners of some small radius of curvature. By increasing the number of terms in the mapping function, rectangles having straight edges and corners of any degree of sharpness can be obtained. The limiting case has stress singularities at the corners.

Figure 5 is a plot of the normalized apparent SIF for rectangular notches corresponding to Figure 3 for elliptical notches. The corresponding curve for the limiting case of a line crack is again a straight line but in this case has a positive slope of unity which results from the fact that $\sigma_0 = \bar{\sigma}$ for uniaxial tension. It should be noted that locally the two solutions have an entirely different character with the rectangular notch having peak stresses at the corners and the ellipse having peak stresses at the notch tip.

A comparison of Figures 3 and 5 shows a remarkable similarity between the elliptical notches with ρ/a = .01 and .05 and the rectangular notches with b/a = .01 and .05. Specifically, it can be seen that the notch curves begin to coincide with the line crack solutions at the same value of r/a whether the notch is elliptical or rectangular if we associate the value of b/a for the rectangular notch with that of ρ/a for the elliptical notch. This implies that it is not the minimum radius of curvature which is important but the relative width of the notch at the tip (note that the rectangular notch has extremely small radii of curvature at the corners and in the limit predicts stress singularities).

As pointed out earlier, the number of terms retained in the mapping function affects the radius of curvature at the corners. Figure 5 represents 10 terms in the mapping function. Figure 6 shows the effect of varying the number of terms on one of the curves of Figure 5. It is obvious that unless a very small number of terms is being used this effect is secondary on the comparison of interest.

The case of angular notches was also studied as a special case of the mapping solution of Appendix A. The character of the solution is somewhat different as illustrated by the sharp tip ($\rho < 5 \times 10^{-3}$mm) rhombus solution shown in Figure 7. Even for very shallow angles the notch solution is seen to be somewhat below the line crack solution. At the origin the curves converge which indicates that the stress intensity factor is the same as that for the line crack. This is further substantiated by the work of Gross and Mendelson [24]. However, away from the origin where experimental data would be gathered the solutions differ by about 10% for a 30° notch. Hence a linear extrapolation would tend to underestimate the stress intensity factor. This effect is partially due to the large value of b/a involved in the rhombus.

The same comparison for a blunted triangular notch is shown in Figure 8. This type of notch is easily obtained in practice by grinding the corners from a standard circular saw blade.

This modification is very useful since the solution behaves essentially like a rectangular notch of width 2ρ rather than $2b$ (compare Figures 5 and 8). As in the previous solution (Figure 7) the notch stresses are somewhat below the crack stresses; however, for $b/a < .10$ the difference is quite acceptable.

FREE BOUNDARY EFFECTS

The effect of a free boundary on the stress field local to a crack

tip has been of considerable interest in the field of fracture mechanics for some years. Numerous analytical and numerical investigations have been carried out with the specific purpose of determining free surface magnification factors for cracks approaching a free boundary. However since the stress intensity factor can be extracted from these solutions with much less labor than a complete solution requires, analytical solutions are limited almost invariably to K_I itself and give no information about higher order terms in the stress components. This causes two significant problems in attempting to verify a crack solution experimentally. First, in the absence of the complete solution, it is impossible to predict a priori the size of the zone dominated by K_I and σ_0 for use in the two parameter techniques previously discussed. Second, it is very difficult to judge whether experimentally observed trends are valid without a knowledge of the qualitative character of the analytical solution away from the crack tip.

Most numerical techniques are not well suited for studying this effect since accurate results are desired in the neighborhood of both a singularity and a free boundary. Therefore any technique which does not make special provision for the singularity or which collocates on the boundary is undesirable.

A convenient geometry for studying this effect is the through crack in a finite width strip shown in Figure 9. Although this problem is two dimensional the qualitative nature of the solution is expected to model very closely the behavior of a three dimensional surface flaw approaching a free boundary since the local behavior of the three dimensional flaw at maximum depth is close to plane strain. Sneddon [25] has reduced the solution of this problem to the solution of the following Fredholm integral equation of the second kind.

$$G(t) = t + t \int_0^{\bar{a}} G(u)H(u,t)du \tag{6}$$

where $\bar{a}$ is the half crack length a nondimensionalized with respect to the half width of the strip w and the kernel is given by:

$$H(u,t) = \int_0^{\infty} \left\{ \frac{xe^{-x}}{\sinh(x)} I_0(xu) I_0(xt) + \frac{2xh(u,x)h(t,x)}{2x + \sinh(2x)} \right\} dx \tag{7}$$

where

$$h(u,x) = [x \coth(x) - 1] I_0(ux) - uxI_1(ux)$$

and I_0 and I_1 are modified Bessel functions of the first kind. This equation has been solved numerically by the method of successive substitutions utilizing a subroutine recommended by Squire [26] for the kernel evaluation. The subroutine is designed for infinite integrals and gives two independent estimates of the integral based on a 20 point Gaussian formula and a 41 point Kronrod rule. The difference between the estimates was of the order of 10^{-7} for this particular integrand and can be taken to be a conservative estimate of the error in the integrand. The technique for solving (6) consisted of splitting the t axis into N discrete points t_j, letting $G_0(t_j) = t_j$ and determining successively G_1, G_2, . . . G_N until convergence was achieved by use of the formula

$$G_{i+1}(t_j) = t_j + t_j \int_0^{\bar{a}} G_i(u) H(u,t_j) du \tag{8}$$

The definite integral was evaluated by a subroutine from [26] very similar to the one previously discussed only for a finite interval. The solution was found to be relatively insensitive to the number of divisions along the t axis. The results for G(t) are plotted in Figure 10 for various values

of a/w. The stress intensity factor is given by $K_I/\bar{\sigma}\,(\pi a)^{1/2} = G(\bar{a})/\bar{a}$ as derived from reference [25]. It was computed for values of a/w ranging from 0.1 to 0.9 and agreed within 1/2% with Sneddon's values.

Having determined G(t) the stresses are obtained by superimposing the following two stress systems as reduced from reference [25].

Stress System I

$$\frac{\bar{\sigma}_x + \bar{\sigma}_y}{2} = \int_0^\infty \phi(\rho) e^{-\rho\bar{y}} \cos(\rho\bar{x})\, d\rho$$

$$\frac{\bar{\sigma}_y - \bar{\sigma}_x}{2} = \bar{y}\int_0^\infty \rho\phi(\rho) e^{-\rho\bar{y}} \cos(\rho x)\, d\rho \qquad (9)$$

$$\bar{\tau}_{xy} = \bar{y}\int_0^\infty \rho\phi(\rho) e^{-\rho\bar{y}} \sin(\rho\bar{x})\, d\rho$$

where $\phi(\rho) = -\rho\int_0^{\bar{a}} G(u)\, J_0(\rho u)\, du$, J_0 is the zeroeth order Bessel function of the first kind, the stresses have been nondimensionalized with respect to the remote stress $\bar{\sigma}$, and $\bar{x}$, $\bar{y}$ are nondimensional coordinates as shown in Figure 9.

Stress System II

$$\frac{\bar{\sigma}_x + \bar{\sigma}_y}{2} = \int_0^\infty g(\rho) \cosh(\rho\bar{x}) \cos(\rho\bar{y})\, d\rho$$

$$\frac{\bar{\sigma}_y - \bar{\sigma}_x}{2} = \int_0^\infty [h(\rho)\cosh(\rho\bar{x}) + \rho\bar{x}\, g(\rho)\sinh(\rho\bar{x})]\cos(\rho\bar{y})\, d\rho \qquad (10)$$

$$\bar{\tau}_{xy} = \int_0^\infty [h(\rho)\sinh(\rho\bar{x}) + \rho\bar{x}\, g(\rho)\cosh(\rho\bar{x})]\sin(\rho\bar{y})\, d\rho$$

where

$$g(\rho) = \frac{\rho}{2\rho + \sinh(2\rho)} \left[2C_2\rho + C_1(3 - 2\rho + e^{-2\rho}) \right]$$

$$h(\rho) = \frac{\rho}{2\rho + \sinh(2\rho)} \left[2C_1(1 - 2\rho + \rho^2 + e^{-2\rho}) + C_2\rho\ (1 - 2\rho + e^{-2\rho}) \right]$$

$$C_1(\rho) = \int_0^{\bar{a}} G(u)\ I_0(\rho u)du$$

$$C_2(\rho) = \int_0^{\bar{a}} G(u)uI_1(\rho u)du$$

and I_0 and I_1 are as previously defined.

Stress system I is singular and for the special case $G(u) = u$ reduces to the solution for a through crack in an infinite body in tension. For this case $\phi(\rho) = -\bar{a}\ J_1(\rho\bar{a})$ which indicates that the integrand in (9) can be expected to be highly oscillatory. In addition, since $e^{-\rho\bar{y}}$ decays very slowly for the region of interest (small $\bar{y}$), it is apparent that a direct numerical approach to this system of equations will be unsatisfactory. Instead an expression of the form

$$G(t) = \sum_{n=1}^{N} A_n t^{2n-1} \qquad (11)$$

was fitted to the numerical values of G(t) by the method of least squares. The use of equation (11) allowed the evaluation of equations (9) in closed form as shown in Appendix B. It also permitted the closed form evaluation of C_1 and C_2 after which stress system II could be evaluated using standard techniques. The integrand of stress system II was also oscillatory due to sine and cosine terms, but it converged quite rapidly due to the term $\sinh(2\rho)$ in the denominator.

Since the solution for G(t) (Figure 10) is nearly linear even for large values of a/w it was found that three terms in (11) were sufficient. The approximation of G(t) had no effect on the free edge boundary conditions $\bar{\sigma}_x(\pm 1,\bar{y}) = \tau_{xy}(\pm 1,\bar{y}) = 0$ since they follow from the form of g and h in equation (10). The shear stress along both planes of symmetry also vanished identically so that the only effect of the approximation was that residual values of $\bar{\sigma}_y$ remained on the crack surface. The average of these residuals varied from 10^{-5}N/mm^2 for a/w = 0.1 to nearly 10^{-2}N/mm^2 for a/w = 0.9. In all cases they are small relative to the applied tension which is unity.

Figure 11 is a nondimensional plot of K_{AP} vs. $r^{1/2}$ based on numerical results of the finite width strip solution. The two parameter singular zone is the linear portion of each curve near the origin. As illustrated by the dashed line passing through the point of tangency drawn from the origin along each curve, the singular zone shrinks rapidly as the crack approaches the free edge of the strip. Perhaps even more significant is the slope of the curves at the origin which is proportional to σ_0. As the crack tip approaches the free boundary the slope increases significantly. This is demonstrated in Figure 12 which is a non-dimensional plot of σ_0 and K_I vs. a/w. It demonstrates that as a/w approaches unity not only is K_I magnified but also σ_0 and that the increase in σ_0 even exceeds that in K_I. This implies that σ_0 is primarily due to the interaction between the singular stress field and the free boundary and has little to do with the remote stress field for problems with near boundaries. This is an important observation for most surface flaw problems of current practical interest which invariably involve free boundaries.

CONCLUSIONS

From this study the following general conclusions can be made:

A - Notch Effects

1) When possible, natural flaws should be used to simulate the line crack. In such cases data gathered outside of $r/a \simeq 10\rho/a$ will ordinarily be free of notch effects.

2) Rectangular notches can be used to simulate line cracks provided that data are gathered outside of some minimum radius. This radius can be judged from the elliptical notch solution (Figure 6) provided that the half width of the rectangular notch is associated with the radius of curvature of the elliptical notch.

3) Blunt triangular notches can be used to simulate the line crack provided that $b/a \leq .10$ and data are gathered outside of a specified value of r/a which can be determined from the elliptical notch solution by associating the half width of the triangular notch at the tip with the radius of curvature of the elliptical notch.

4) Sharp angular notches will tend to significantly underestimate the stress intensity factor unless data are taken extremely close in.

B - Free Boundary Effects

5) The singular zone is shown to shrink rapidly as a crack approaches the free edge of a strip.

6) When a crack is near a free boundary, σ_0 depends primarily upon the interaction between the singular stress field and the free boundary, and is not strongly influenced by the remote stress.

All of the foregoing conclusions are specifically directed towards clarifying the determination of SIF values by means of the TSCM utilizing stress freezing photoelasticity which involves no plastic zone. However, there is a very local non-linear region [21] which is expected to produce effects in

the singular zone which would be similar to those associated with small scale yielding in structural materials.

ACKNOWLEDGEMENTS

The authors wish to acknowledge the assistance of G. W. Swift in formulating suitable computer programs, the staff and facilities of the Engineering Science and Mechanics Department at VPI & SU and the support of the Department of Defense, U.S. Army, under contract No. DAA-F07-69-C-0444 with Watervliet Arsenal.

APPENDIX A

MAPPING SOLUTION

It is well known that the stresses around a hole in a homogeneous isotropic plate can be obtained by the complex variable technique introduced by Muskhelishvili [23]. Numerous problems involving square, rectangular and triangular holes have been solved by Savin [22]. For the most part these solutions contain only a few terms in the series expansion of the mapping function and hence involve curvilinear sides and rounded off corners. With the advent of the digital computer it has become feasible to automate the process of determining the Muskhelishvili potentials ϕ and ψ and hence to arrive at solutions containing arbitrarily sharp corners and straight edges. Thus it is possible to determine the effect of the geometrical approximations involved in truncating the series mapping function.

For the present purpose of determining the effect of various types of notches on the estimation of the mode I stress intensity factor it is desirable to consider the axisymmetric eight sided polygon of Figure A-1. Once the general solution is obtained for this region the following special cases can be evaluated:

a) Rectangular notch ($\alpha = 0$, $\phi_1 = \phi_2 \neq 0$)

b) Rhombus ($\alpha \neq 0$, $\phi_1 = 0$, $\phi_2 = \frac{\pi}{2}$)

c) Rectangular notch with sharp triangular tip

($\alpha \neq 0$, $\phi_1 = 0$, $\phi_2 \neq 0$)

d) Rectangular notch with blunted triangular tip

($\alpha \neq 0$, $\phi_1 \neq 0$, $\phi_2 \neq 0$)

To obtain the mapping of Figure A-1, the Schwartz Christoffel transformation is first applied which maps the exterior of the polygon in the z plane into the exterior of the unit circle in the ζ plane. This transformation is given by (see [22])

$$z = R \int^{\zeta} \left(1 - \frac{A'}{t}\right)^{\alpha_1 - 1} \left(1 - \frac{B'}{t}\right)^{\alpha_2 - 1} \cdots \left(1 - \frac{H'}{t}\right)^{\alpha_8 - 1} dt$$

$$+ \text{complex constant.} \qquad \text{(A-1)}$$

Referring to Figure A-1 it is apparent from symmetry considerations that

$$A' = -E' = e^{-i\phi_1}$$

$$B' = -F' = e^{-i\phi_2}$$

$$C' = -G' = \overline{F}' = -e^{i\phi_2}$$

$$D' = -H' = \overline{E}' = -e^{i\phi_1}$$

and

$$\alpha_1 = \alpha_4 = \alpha_5 = \alpha_8 = \frac{3-\alpha}{2}$$

$$\alpha_2 = \alpha_3 = \alpha_6 = \alpha_7 = \frac{1+\alpha}{2}$$

Hence equation (A-1) takes the form

$$z = R \int^{\zeta} \left(1 - \frac{e^{-2i\phi_1}}{t^2}\right)^{(1-\alpha)/2} \left(1 - \frac{e^{2i\phi_1}}{t^2}\right)^{\alpha/2} \left(1 - \frac{e^{-2i\phi_2}}{t^2}\right)^{(1-\alpha)/2}$$

$$\left(1 - \frac{e^{2i\phi_2}}{t^2}\right)^{\frac{\alpha}{2}} dt + \text{complex constant.} \qquad \text{(A-2)}$$

Since $|e^{i\theta}| = 1$ and $|t| \geq 1$, this equation can be approximated by expanding each of the factors in a binomial series and multiplying the resulting polynomials. Then by integrating the resulting polynomial and by inversion (i.e. by replacing ζ by $\frac{1}{\zeta}$) the desired mapping is obtained.

As a result of symmetry it is found that the required mapping is of the form

$$z = R\left[\frac{1}{\zeta} + \sum_{n=1}^{N} C_n \zeta^{2n-1}\right] = \omega(\zeta) \qquad \text{(A-3)}$$

where the coefficients R, C_n are real and the expansion has been truncated after the Nth term. A computer program was written to carry out the above calculations for given values of ϕ_1, ϕ_2, α and N.

It is well known that the solution of the first boundary value problem of elasticity can be reduced to the determination of two analytic functions $\phi(z)$ and $\psi(z)$ of the complex variable z. The stresses are related to the complex potentials ϕ and ψ by the following formulae where primes denote differentiation:

$$\sigma_x + \sigma_y = 2[\phi'(z) + \overline{\phi}'(z)]$$

$$\sigma_y - \sigma_x + 2i\tau_{xy} = 2[\overline{z}\phi''(z) + \psi'(z)] \qquad \text{(A-4)}$$

The stress boundary conditions using this formulation take the form

$$\phi(z) + z\overline{\phi}'(z) + \overline{\psi}(z) = f_1 + if_2 \text{ on } C \tag{A-5}$$

where $f_1 + if_2 = i\int_{s_0}^{s} [T_1(s) + iT_2(s)]\, ds$ is the force transmitted across a segment of the boundary (ds) and T_1, T_2 are components of the applied tractions on the boundary C. Under the transformation $z = \omega(\zeta)$ (using the notation $\phi(\delta) = \phi(\omega(\zeta))$ etc.) the stress transformation equations yield the following expressions for the stress components σ_ρ, $\tau_{\rho\phi}$, σ_ϕ in the curvilinear coordinate system corresponding to the contour lines ρ = constant and ϕ = constant where $z = \omega(\rho e^{i\phi})$.

$$\begin{aligned} \sigma_\rho + \sigma_\phi &= 2[\phi(\zeta) + \overline{\phi}(\zeta)] \\ \sigma_\phi - \sigma_\rho + 2i\tau_{\rho\phi} &= \frac{2\zeta^2}{\rho^2 \overline{\omega}'(\zeta)} [\overline{\omega}(\zeta)\, \phi'(\zeta) + \omega'(\zeta)\psi(\zeta)] \end{aligned} \tag{A-6}$$

The stress functions ϕ and ψ can be separated into components ϕ^*, ψ^* representing the stress state in the absence of the hole and ϕ_0, ψ_0 due to the presence of the hole. For uniaxial tension in the y direction ϕ^* and ψ^* take the form

$$\begin{aligned} \phi^* &= \frac{\overline{\sigma z}}{4} = \frac{\overline{\sigma}}{4}\omega(\zeta) \\ \psi^* &= \frac{\overline{\sigma z}}{2} = \frac{\overline{\sigma}}{2}\omega(\zeta) \end{aligned} \tag{A-7}$$

The potentials ϕ_0 and ψ_0 can be expanded as follows (where only odd powers need be retained due to symmetry in both region and loading):

$$\phi_o = \sum_{n=1}^{\infty} A_n \zeta^{2n-1} \qquad \psi_o = \sum_{n=1}^{\infty} B_n \zeta^{2n-1} \tag{A-8}$$

As first shown by Muskhelishvili [23] the boundary conditions can be written in terms of the two functional equations:

$$\begin{aligned} \phi_o(\zeta) + \frac{1}{2\pi i}\int_\Gamma \frac{\omega(\hat{\sigma})}{\overline{\omega}'(\hat{\sigma})}\,\overline{\phi}_o'(\hat{\sigma})\,\frac{d\hat{\sigma}}{\hat{\sigma}-\zeta} + \overline{B}_o &= \frac{1}{2\pi i}\int_\Gamma \frac{f_1 + if_2}{\hat{\sigma}-\zeta}\,d\hat{\sigma} \\ \psi_o(\zeta) + \frac{1}{2\pi i}\int_\Gamma \frac{\overline{\omega}(\hat{\sigma})}{\omega'(\hat{\sigma})}\,\phi_o'\,\frac{d\hat{\sigma}}{\hat{\sigma}-\zeta} &= \frac{1}{2\pi i}\int_\Gamma \frac{f_1 - if_2}{\hat{\sigma}-\zeta}\,d\hat{\sigma} \end{aligned} \tag{A-9}$$

where Γ represents the unit circle. For uniaxial tension in the y direction it can be shown that (see [22]):

$$\begin{aligned} f_2 &= 0 \\ f_1 &= \frac{-\overline{\sigma}}{2}\left[\omega(\hat{\sigma}) + \overline{\omega}(\hat{\sigma})\right] \end{aligned} \tag{A-10}$$

Substituting (A-3) in (A-10) and noting that the mapping coefficients are real yields:

$$f_1 = \frac{-\overline{\sigma}R}{2}\left[\frac{1}{\hat{\sigma}} + \sum_{n=1}^{N} C_n \hat{\sigma}^{2n-1} + \frac{1}{\overline{\hat{\sigma}}} + \sum_{n=1}^{N} C_n \overline{\hat{\sigma}}^{\,2n-1}\right] \tag{A-11}$$

But $\overline{\hat{\sigma}} = \overline{\hat{\sigma}}^{-1}$; hence (A-11) becomes

$$f_1 = -\frac{\overline{\sigma}R}{2}\left[\frac{1}{\hat{\sigma}} + \hat{\sigma} + \sum_{n=1}^{N} C_n(\hat{\sigma}^{2n-1} + \hat{\sigma}^{1-2n})\right] \tag{A-12}$$

Hence the right hand side of equation (A-9) becomes

$$\frac{1}{2\pi i}\int_{\Gamma}\frac{f_1 d\hat{\sigma}}{\hat{\sigma}-\zeta} = -\frac{\overline{\sigma R}}{2}\left[\zeta + \sum_{n=1}^{N} C_n \zeta^{2n-1}\right] \tag{A-13}$$

where the following result from the theory of residues has been used:

$$\frac{1}{2\pi i}\int_{\Gamma}\frac{\hat{\sigma}^n d\hat{\sigma}}{\hat{\sigma}-\zeta} = \begin{cases} \zeta^n & n \geq 0 \\ 0 & n < 0 \end{cases} \tag{A-14}$$

Utilizing equation (A-3) and noting that $\omega'(\hat{\sigma}) \neq 0$ and hence $\overline{\omega}'(\hat{\sigma}) \neq 0$ for single valued mapping functions we obtain the identity:

$$\frac{\omega(\hat{\sigma})}{\overline{\omega}'(\hat{\sigma})} = \frac{\frac{1}{\hat{\sigma}} + \sum_{n=1}^{N} C_n \hat{\sigma}^{2n-1}}{\frac{-1}{\hat{\sigma}^2} + \sum_{n=1}^{N}(2n-1)C_n\hat{\sigma}^{2-2n}} = \sum_{n=1}^{N-1} H_n \hat{\sigma}^{2n-1}$$

$$+ \text{ negative powers of } \hat{\sigma} \tag{A-15}$$

where the H's are obtained by long division and negative powers of $\hat{\sigma}$ are unnecessary because they do not contribute to the Cauchy integrals. Also from equation (A-8) we have

$$\overline{\phi}_o'(\hat{\sigma}) = \sum_{n=1}^{\infty}(2n-1)\,\overline{A}_n\hat{\sigma}^{2-2n} \tag{A-16}$$

Multiplying equations (A-15) and (A-16) yields

$$\frac{\omega(\hat{\sigma})}{\overline{\omega}'(\hat{\sigma})}\overline{\phi}_o'(\hat{\sigma}) = \sum_{n=1}^{N-1} K_n\hat{\sigma}^{2n-1} + \text{negative powers of } \sigma \tag{A-17}$$

where K_i and A_i are related by the matrix equation:

$$K_i = B_{ij}\,\bar{A}_j \quad \text{(implied summation)} \tag{A-18}$$

and the coefficient matrix is given by

$$B_{ij} = (2j-1)\,H_{i+j-1} \quad \text{(no summation)}. \tag{A-19}$$

Making use again of relation (A-14) the second term in the first of equation (A-9) becomes

$$\frac{1}{2\pi i}\int_{\Gamma}\sum_{n=1}^{N-1} K_n\hat{\sigma}^{2n-1}\,\frac{d\hat{\sigma}}{\hat{\sigma}-\zeta} = \sum_{n=1}^{N-1} K_n\zeta^{2n-1} = \sum_{n=1}^{N-1} B_{nj}\bar{A}_j\zeta^{2n-1} \tag{A-20}$$

Substituting equations (A-8), (A-13), and (A-20) in the first of (A-9) yields the result that $B_0 = 0$ and provides the following system of equations to solve for the A_n:

$$\begin{aligned} A_1 + B_{1j}\,\bar{A}_j &= -\frac{\bar{\sigma}R}{2}\,[1 + C_1] \\ A_n + B_{nj}\,\bar{A}_j &= -\frac{\bar{\sigma}R}{2}\,C_n \qquad n = 2, 3, \ldots N-1 \\ A_N &= -\frac{\bar{\sigma}R}{2}\,C_N \end{aligned} \tag{A-21}$$

Since the mapping coefficients C_n are real for the cases to be investigated here the coefficients A_n will obviously be real also. Hence equation (A-21) can be written in the concise form

$$\begin{aligned} (\delta_{nj} + B_{nj})\,A_j &= -\frac{\bar{\sigma}R}{2}\,[\delta_{1n} + C_n] \qquad n = 1, N-1 \\ A_N &= -\frac{\bar{\sigma}R}{2}\,C_N \end{aligned} \tag{A-22}$$

where δ_{ij} is the Kronecker delta.

Once ϕ_o is known ψ_o can be determined from the second of equations (A-9) which can be reduced to the following form (see Sokolnikoff [28], equation 84.11):

$$\psi_o(\zeta) = \frac{1}{2\pi i}\int_\Gamma \frac{f_1 - if_2}{\hat{\sigma} - \zeta}\, d\hat{\sigma} - \frac{\overline{\omega}^*(1/\zeta)}{\omega'(\zeta)}\,\phi_o'(\zeta) + \sum_{n=1}^{N-1} \overline{K}_n \zeta^{1-2n} \qquad \text{(A-23)}$$

where for real coefficients $\overline{K}_n = K_n$ and

$$\overline{\omega}^*(\zeta) = \overline{R}\left[\frac{1}{\zeta} + \sum_{n=1}^{N} \overline{C}_n \zeta^{2n-1}\right] = \omega(\delta)$$

Substituting equations (A-3), (A-8), and (A-13) in (A-23) we obtain finally:

$$\psi_o(\zeta) = -\frac{\overline{\sigma R}}{2}\left[\zeta + \sum_{n=1}^{N} C_n \zeta^{2n-1}\right] + \sum_{n=1}^{N-1} K_n \zeta^{1-2n}$$

$$+ \frac{\zeta + \sum_{n=1}^{N} C_n \zeta^{1-2n}}{\frac{1}{\zeta^2} - \sum_{n=1}^{N} (2n-1)\, C_n \zeta^{2n-2}}\left[\sum_{n=1}^{N} (2n-1)\, A_n \zeta^{2n-2}\right] \qquad \text{(A-24)}$$

This completes the formal solution. The previous calculations were programmed for a digital computer which computed ϕ, ψ given the coefficients in the mapping function and proceeded to evaluate the stresses according to equations (A-4) and (A-6).

APPENDIX B

EVALUATION OF STRESS SYSTEM 1

Substituting the definition for $\phi(\rho)$ in equations (9), interchanging the order of integration, and noting that $e^{i\rho\bar{z}} = e^{-\rho\bar{y}}[\cos(\rho\bar{x}) + i \sin(\rho\bar{x})]$ yields the following (where $\bar{z} = \bar{x} + i\,\bar{y}$ is a nondimensional variable, not a complex conjugate):

$$\frac{\bar{\sigma}_x + \bar{\sigma}_y}{2} = - \mathrm{Re} \int_0^{\bar{a}} G(u) \int_0^{\infty} \rho\, J_0(\rho u) e^{i\rho\bar{z}}\, d\rho\, du$$

$$\frac{\bar{\sigma}_y - \bar{\sigma}_x}{2} = - \mathrm{Re} \int_0^{\bar{a}} G(u) \int_0^{\infty} \rho^2 J_0(\rho u) e^{i\rho\bar{z}}\, d\rho\, du \qquad \text{(B-1)}$$

$$\bar{\tau}_{xy} = - \mathrm{Im} \int_0^{\bar{a}} G(u) \int_0^{\infty} \rho^2 J_0(\rho u) e^{i\rho\bar{z}}\, d\rho\, du$$

The inner integrals can be evaluated by noting the following identities

$$\int_0^{\infty} \rho J_0(\rho u) e^{i\rho\bar{z}}\, d\rho = - i \frac{d}{d\bar{z}} \int_0^{\infty} J_0(\rho u) e^{i\rho\bar{z}}\, d\rho = - i \frac{d}{d\bar{z}} (u^2 - \bar{z}^2)^{-\frac{1}{2}}$$

$$\text{(B-2)}$$

$$\int_0^{\infty} \rho^2 J_0(\rho u) e^{-i\rho\bar{z}}\, d\rho = - \frac{d^2}{d\bar{z}^2} \int_0^{\infty} J_0(\rho u) e^{i\rho\bar{z}}\, d\rho = - \frac{d^2}{d\bar{z}^2} (u^2 - \bar{z}^2)^{-\frac{1}{2}}$$

where the second integral has been evaluated using the following result from a table of Laplace transforms.

$$\int_0^\infty e^{-st} J_0(at)\, dt = \frac{1}{\sqrt{s^2+a^2}} \tag{B-3}$$

Substituting (B-2) in (B-1) yields the following:

$$\frac{\bar{\sigma}_x + \bar{\sigma}_y}{2} = \text{Re } i \frac{d}{d\bar{z}} \int_0^{\bar{a}} \frac{G(u)\, du}{\sqrt{u^2-\bar{z}^2}}$$

$$\frac{\bar{\sigma}_y - \bar{\sigma}_x}{2} = \bar{y}\ \text{Re} \frac{d^2}{d\bar{z}^2} \int_0^{\bar{a}} \frac{G(u)\, du}{\sqrt{u^2-\bar{z}^2}} \tag{B-4}$$

$$\bar{\tau}_{xy} = \bar{y}\ \text{Im} \frac{d^2}{d\bar{z}^2} \int_0^{\bar{a}} \frac{G(u)\, du}{\sqrt{u^2-\bar{z}^2}}$$

Equations (B-4) can be reduced to the well known Westergaard formulation [27] for which the stresses are given by:

$$\begin{aligned} \bar{\sigma}_x &= \text{Re } Z - \bar{y}\ \text{Im } Z' \\ \bar{\sigma}_y &= \text{Re } Z + \bar{y}\ \text{Im } Z' \\ \bar{\tau}_{xy} &= -\bar{y}\ \text{Re } Z' \end{aligned} \tag{B-5}$$

by defining Z in the following manner:

$$Z = i \frac{d}{d\bar{z}} \int_0^{\bar{a}} \frac{G(u)\, du}{\sqrt{u^2-\bar{z}^2}} \tag{B-6}$$

Substituting equation (11) with N = 3 for G(t) in (B-6) and carrying out the necessary integrations yields the following expression for Z.

$$Z = \frac{\alpha_1 \bar{z}}{\sqrt{\bar{z}^2 - \bar{a}^2}} + \alpha_2 \sqrt{\bar{z}^2 - \bar{a}^2} - A_1 - 2A_3 \bar{z}^2 - \frac{8}{3} A_5 \bar{z}^4 \qquad \text{(B-7)}$$

where $\alpha_1 = A_1 + A_3 (2\bar{z}^2 + \bar{a}^2)/3 + A_5 (3\bar{a}^4 + 4\bar{a}^2\bar{z}^2 + 8\bar{z}^4)/15$

$\alpha_2 = (20A_3 \bar{z} + 8A_5 \bar{a}^2\bar{z} + 32A_5 \bar{z}^3)/15$

For the limiting case of a through crack in an infinite body, $A_1 = 1$, $A_2 = A_3 = 0$ and (B-7) reduces to

$$Z = \frac{\bar{z}}{\sqrt{\bar{z}^2 - \bar{a}^2}} - 1 \qquad \text{(B-8)}$$

which agrees with the Westergaard solution [27].

REFERENCES

[1] Irwin, G. R., Discussion of the Paper, "The Dynamic Stress Distribution Surrounding a Running Crack," by A. A. Wells and D. Post, Proceedings, Society for Experimental Stress Analysis, 16, 1, pp. 69-92 (1958).

[2] Fessler, H. and Mansell, D. O., "Photoelastic Study of Stresses Near Cracks in Thick Plates," Journal of Mechanical Engineering Science, 4, 3, pp. 213-225 (1962).

[3] Marloff, R. H., Leven, M. M., Johnson, R. L. and Ringler, T. N., "Photoelastic Determination of Stress Intensity Factors," Experimental Mechanics, 11, 12, pp. 529-539 (Dec. 1971).

[4] Bradley, W. B. and Kobayashi, A. S., "An Investigation of Propagating Cracks by Dynamic Photoelasticity," J. of Experimental Mechanics, 10, 3, pp. 106-113, (March 1970).

[5] Bradley, W. B. and Kobayashi, A. S., "Fracture Dynamics - A Photoelastic Investigation," J. of Engineering Fracture Mechanics, 3, 3, pp. 317-332 (Oct. 1971).

[6] Kobayashi, A. S. and Wade, B. G., "Crack Propagation and Arrest in Impacted Plates," TR-14, Department of Mechanical Engineering, University of Washington, Seattle, Wash. (July 1972).

[7] Liebowitz, H., Vanderveldt, H., and Sanford, R.J., "Stress Concentrations Due to Sharp Notches," Experimental Mechanics, 7, pp. 513-517 (1967).

[8] Smith D. G. and Smith, C. W., "Photoelastic Determination of Mixed Mode Stress Intensity Factors," J. of Engineering Fracture Mechanics, 4, 2, pp. 357-366 (June 1972).

[9] Smith, D. G. and Smith, C. W., "A Photoelastic Evaluation of the Influence of Closure and Other Effects Upon the Local Bending Stresses in Cracked Plates," International Journal of Fracture Mechanics, 6, 3, pp. 305-318 (Sept. 1970).

[10] Marrs, G. R. and Smith, C. W., "A Study of Local Stresses Near Surface Flaws in Bending Fields," Stress Analysis and Growth of Cracks, ASTM STP 513, pp. 22-36 (Oct. 1972).

[11] Smith, D. G. and Smith, C. W., "Influence of Precatastrophic Extension and Other Effects on Local Stresses in Cracked Plates Under Bending Fields," Experimental Mechanics, 11, 9, pp. 394-401 (Sept. 1971).

[12] Schroedl, M. A., McGowan, J. J. and Smith, C. W., "An Assessment of Factors Influencing Data Obtained by the Photoelastic Stress Freezing Technique for Stress Fields Near Crack Tips," J. of Engineering Fracture Mechanics, 4, 4, pp. 801-809 (Dec. 1972).

[13] Schroedl, M. A. and Smith, C. W., "Local Stresses Near Deep Surface Flaws Under Cylindrical Bending Fields," VPI-E-72-9, Progress in Flaw Growth and Fracture Toughness Testing, ASTM STP 536, pp. 45-63 (Oct. 1973).

[14] Schroedl, M. A., McGowan, J. J. and Smith, C. W., "Determination of Stress Intensity Factors From Photoelastic Data with Application to Surface Flaw Problems," VPI-E-73-1, (Feb. 1973), (In Press) J. of Experimental Mechanics.

[15] Harms, A. E. and Smith, C. W., "Stress Intensity Factors in Long Deep Surface Flaws in Plates Under Extensional Fields," VPI-E-73-6 (Feb. 1973), Tenth Anniversary Meeting of Society for Engineering Science, Raleigh, N. C. (Nov. 1973).

[16] Schroedl, M. A. and Smith, C. W., "Influence of Three Dimensional Effects on the Stress Intensity Factor for Compact Tension Specimens", VPI-E-73-15, 20 pages, (April 1973), (In Press) Fracture [redacted] Anal. ASTM STP [redacted] 560.

[17] Schroedl, M. A., McGowan, J. J. and Smith, C. W., "Use of a Taylor Series Correction Method in Photoelastic Stress Intensity Determinations," VPI-E-73-34 (1973), Spring Meeting SESA Detroit, Mich. (May 1974).

[18] Mullinix, B. R. and Smith, C. W., "Distribution of Local Stresses Across the Thickness of Cracked Plates Under Bending Fields," (In Press) International Journal of Fracture Mechanics (1974).

[19] McGowan, J. J. and Smith, C. W., "Stress Intensity Factors for Deep Cracks Emanating from the Corner Formed by a Hole Intersecting a Plate Surface," VPI-E-74-1 (1974).

[20] Smith, C. W., "Use of Three Dimensional Photoelasticity in Fracture Mechanics," (Invited Paper) Third International Congress on Experimental Mechanics, Los Angeles, Calif., May 13-18, 1973 (In Press), Conference Proceedings and J. of Experimental Mechanics, 13, 12, pp. 539-544 (Dec. 1973).

[21] McGowan, J. J. and Smith, C. W., "A Finite Deformation Analysis of the Near Field Surrounding the Tip of Small Crack-Like Ellipses," VPI-E-74-10 (1974).

[22] Savin, C. N., Stress Concentrations Around Holes, Pergamon Press, pp. 9-14 (1974).

[23] Muskhelishvili, M. I., Some Basic Problems of the Mathematical Theory of Elasticity, Noordhoff, (1953).

[24] Gross, B. and Mendelson, A., "Plane Elasto-Static Analysis of V-Notched Plates," International Journal of Fracture Mechanics, 8, 3, pp. 267-276 (Sept. 1972).

[25] Sneddon, I. N. and Srivastav, R. P., "The Stress Field in the Vicinity of a Griffith Crack in a Strip of Finite Width," Int. J. Eng. Sci., 9, pp. 279-488 (1971).

[26] Squire, W., Integration for Engineers and Scienticists, American Elsevier Publishing Company, Inc., New York, p. 279 (1970).

[27] Westergaard, H. M., "Bearing Pressures on Cracks," Trans. ASME (1939).

[28] Sokolnikoff, I. S., Mathematical Theory of Elasticity, Second Edition, McGraw-Hill Book Co., New York (1956).

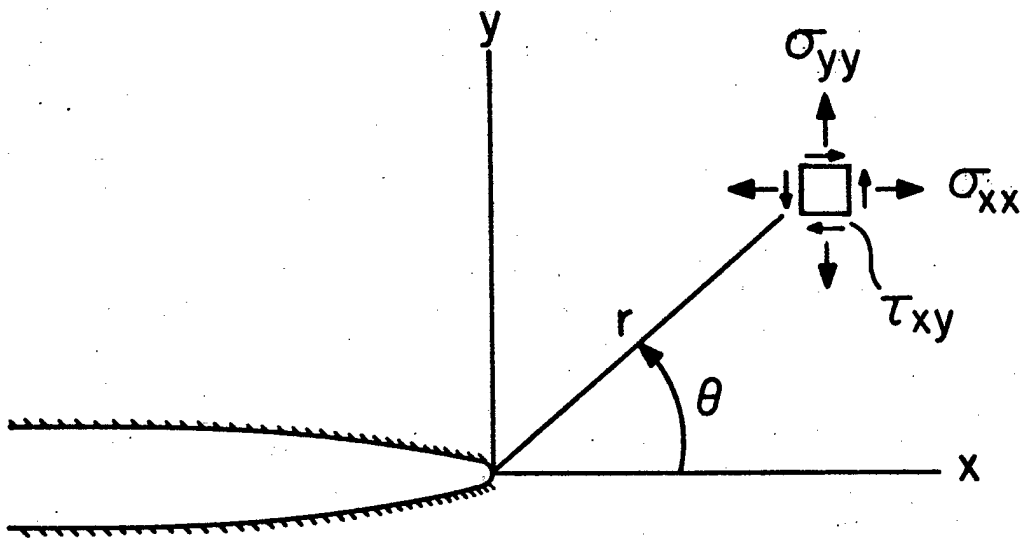

Figure 1. Singular Stress Notation

Figure 2. Microphoto of Naturally Grown Flaw.

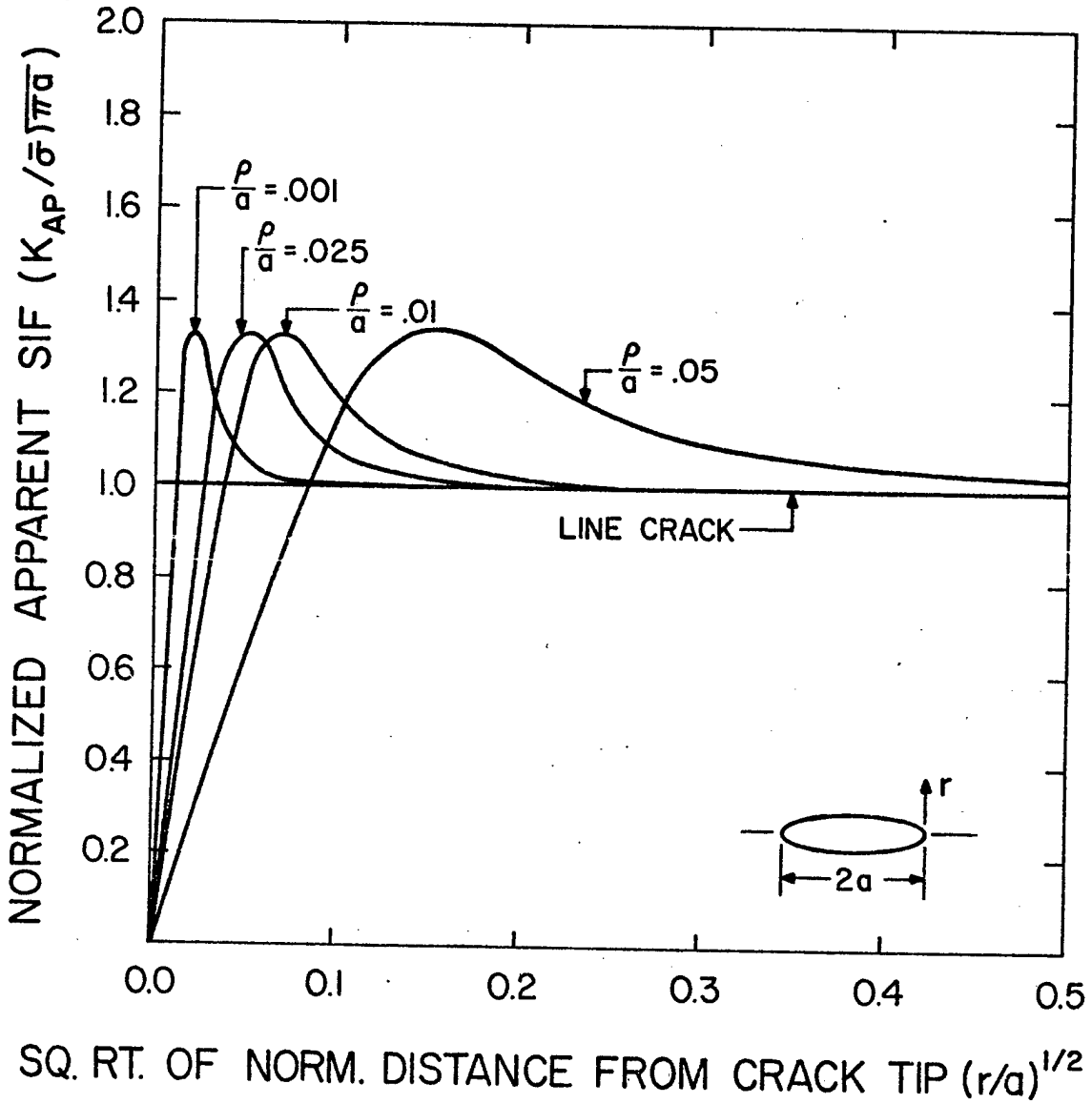

Figure 3. Results of Elliptical Notch Comparison.

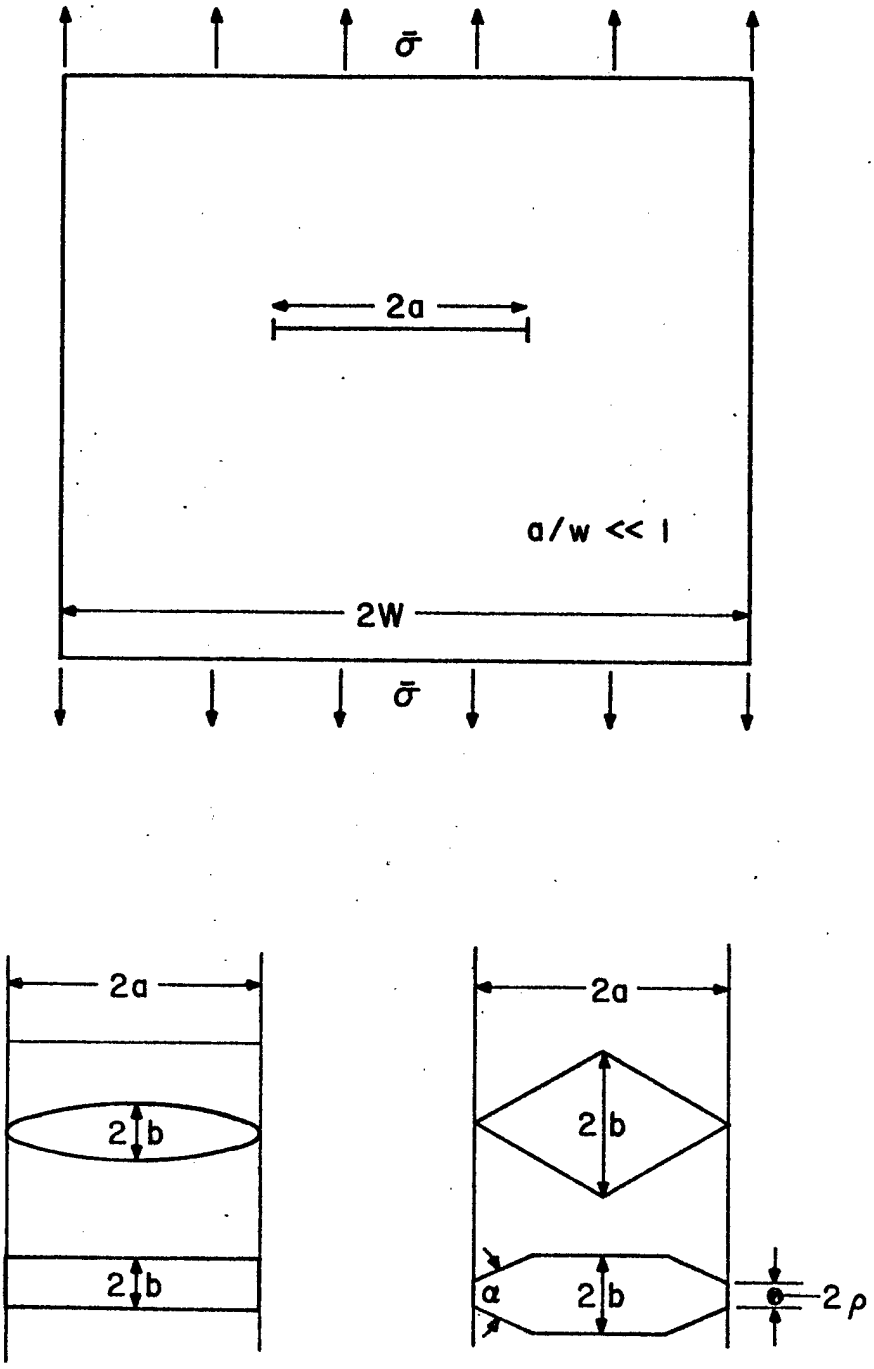

Figure 4. Geometries to be Used in Notch Crack Comparison.

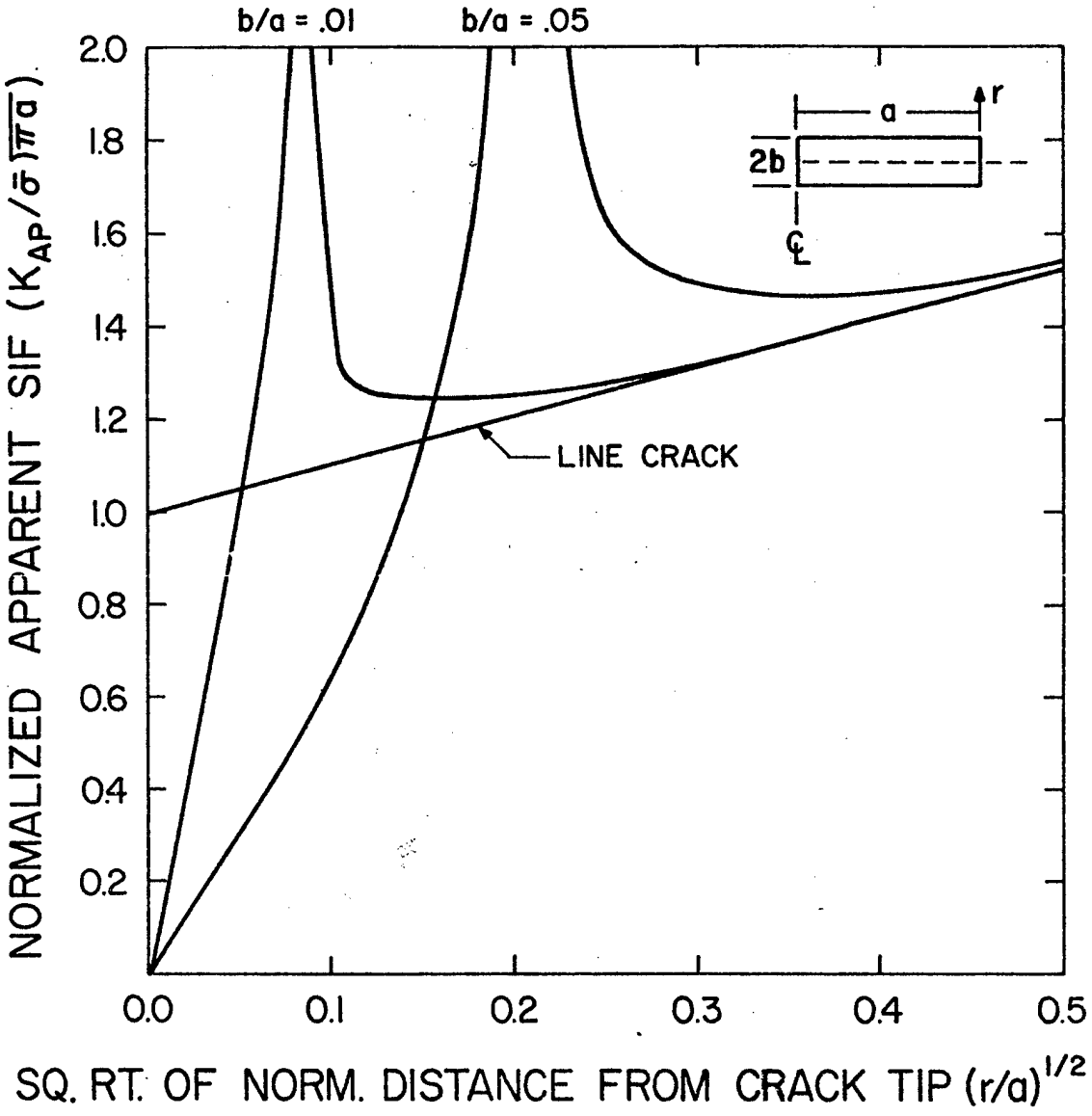

Figure 5. Results of Rectangular Notch Comparison.

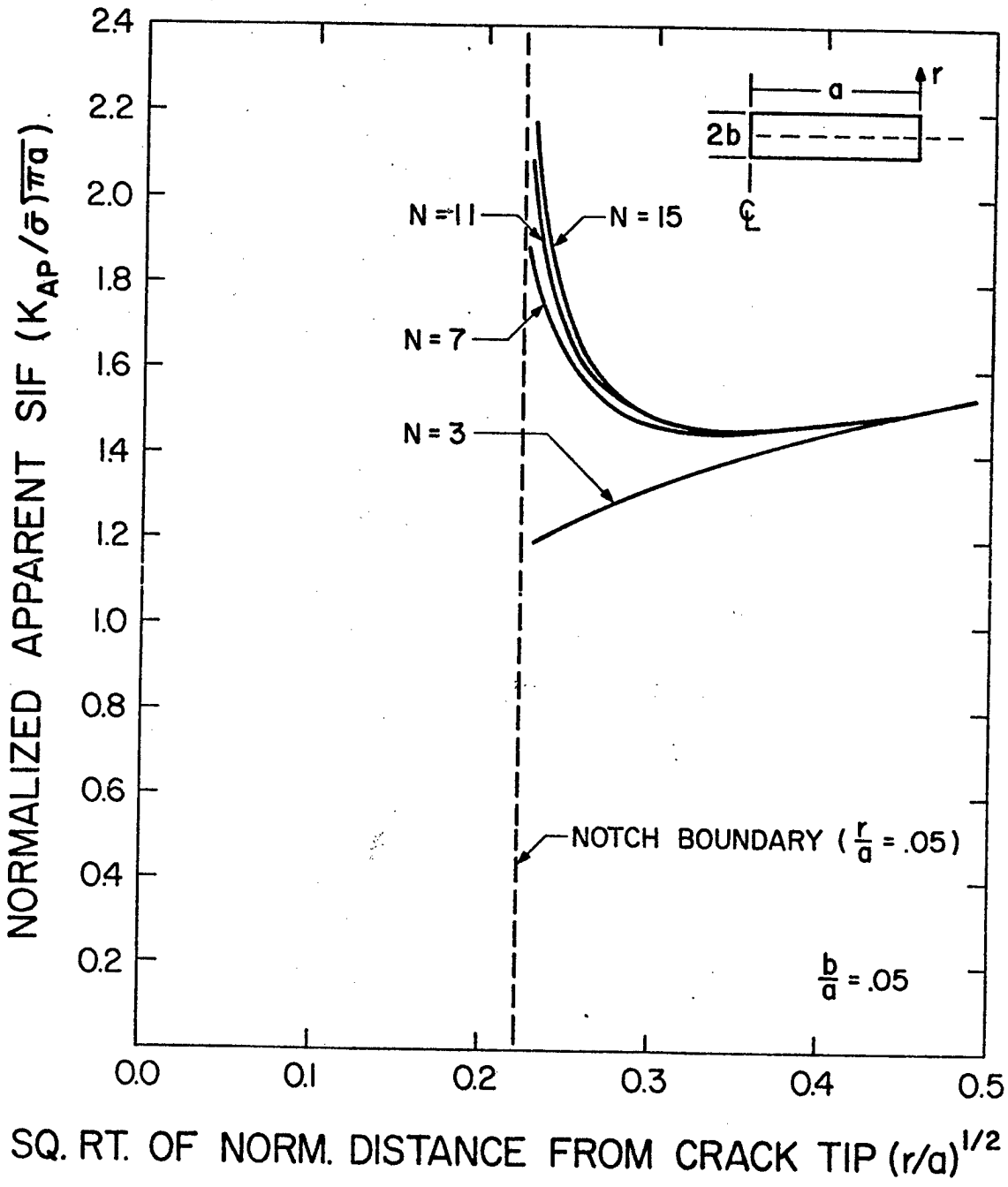

Figure 6. Effect of Number of Terms on Rectangular Notch Solution.

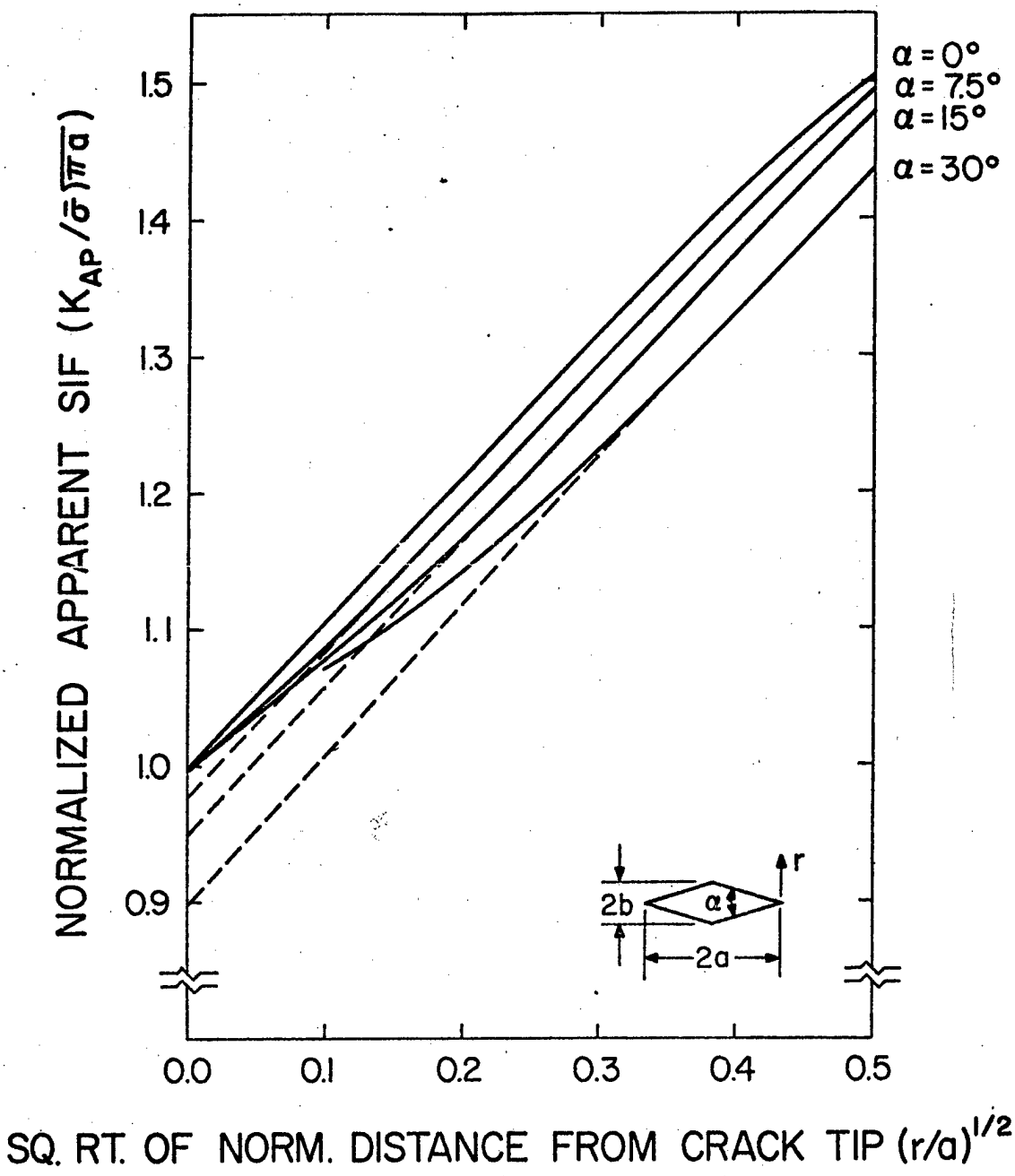

Figure 7. Results of Rhombus Comparison.

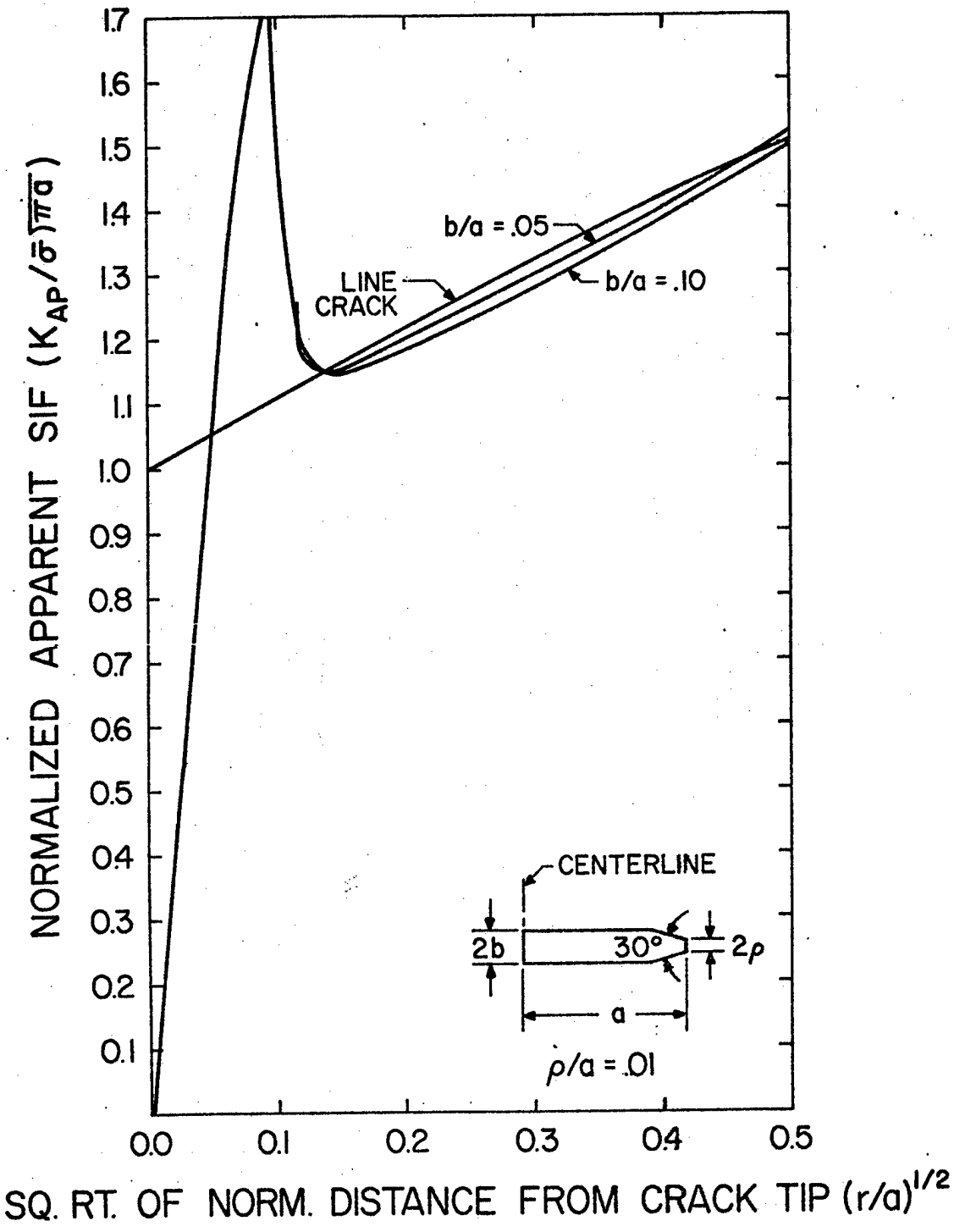

Figure 8. Results of Blunted Triangular Notch Comparison.

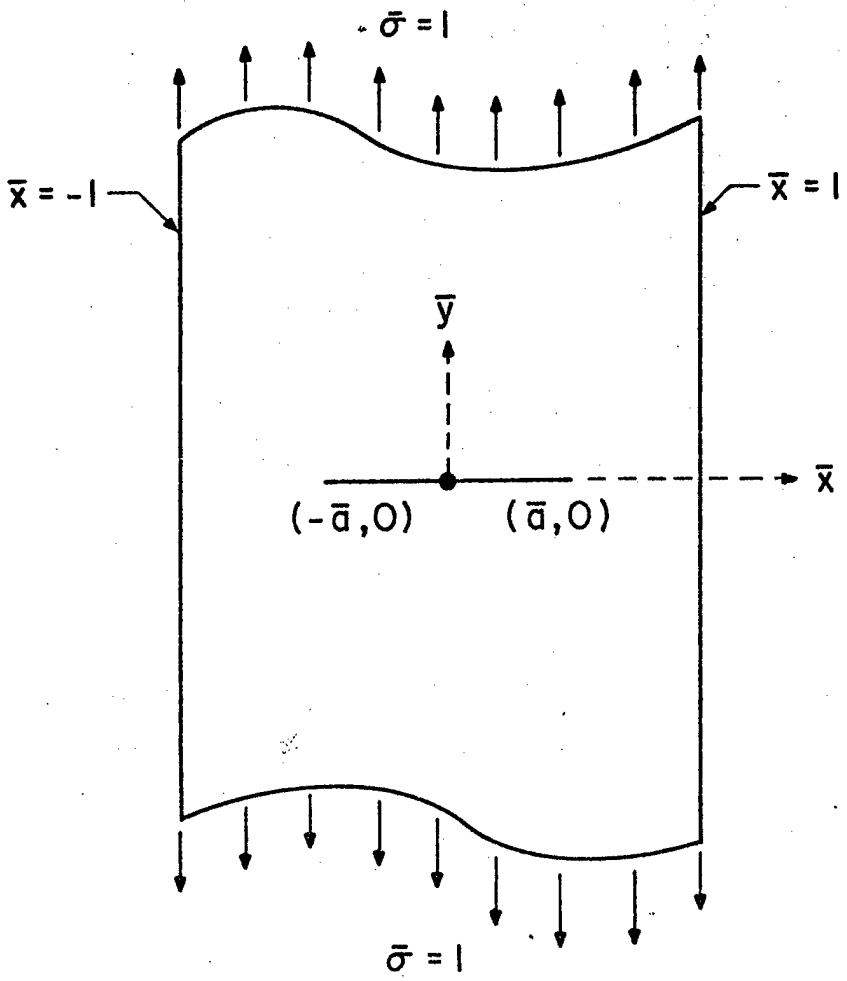

Figure 9. Crack Geometry for Studying Free Boundary Effect.

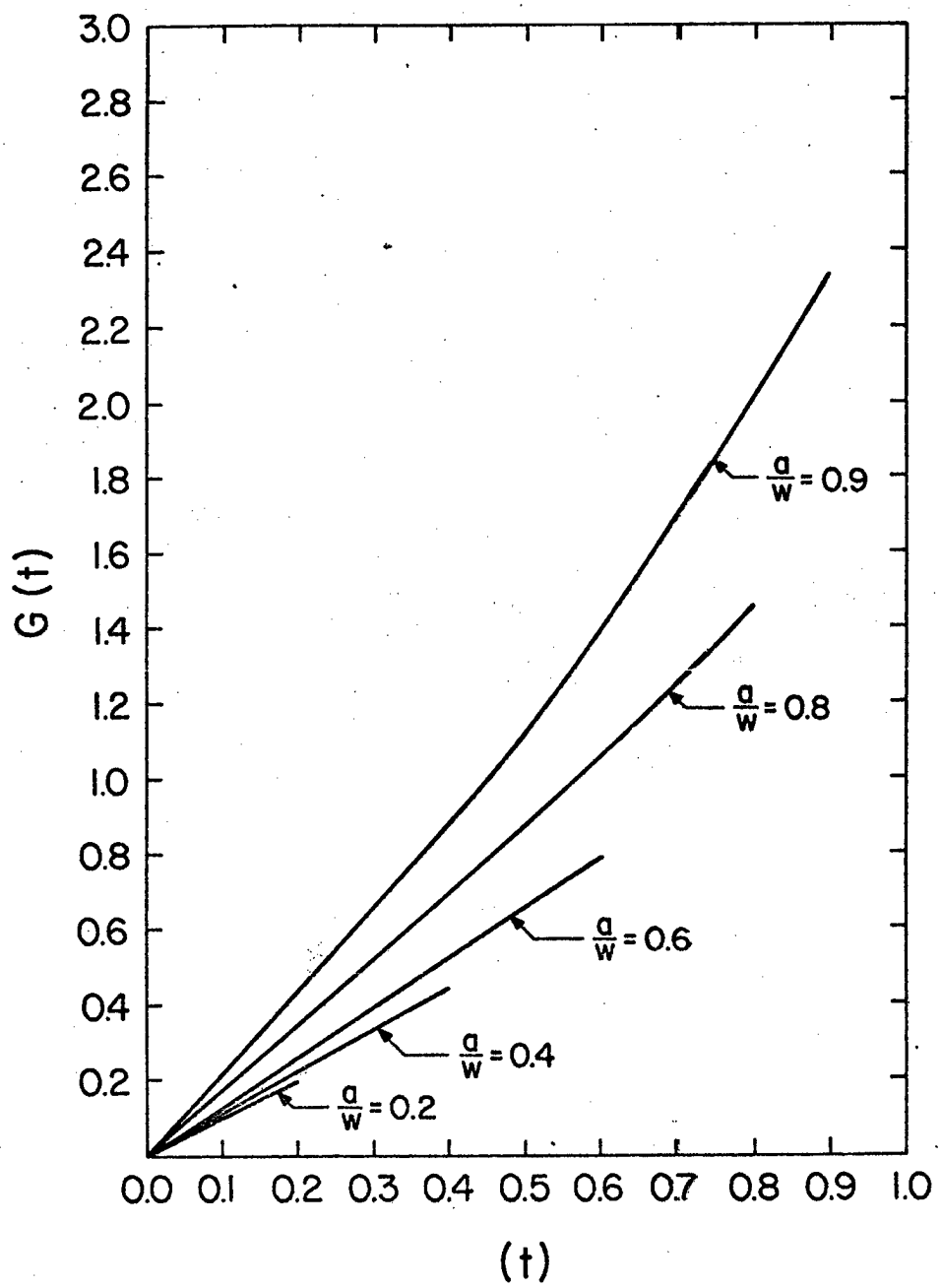

Figure 10. Solution for G(t) for Through Crack in Finite Width Strip.

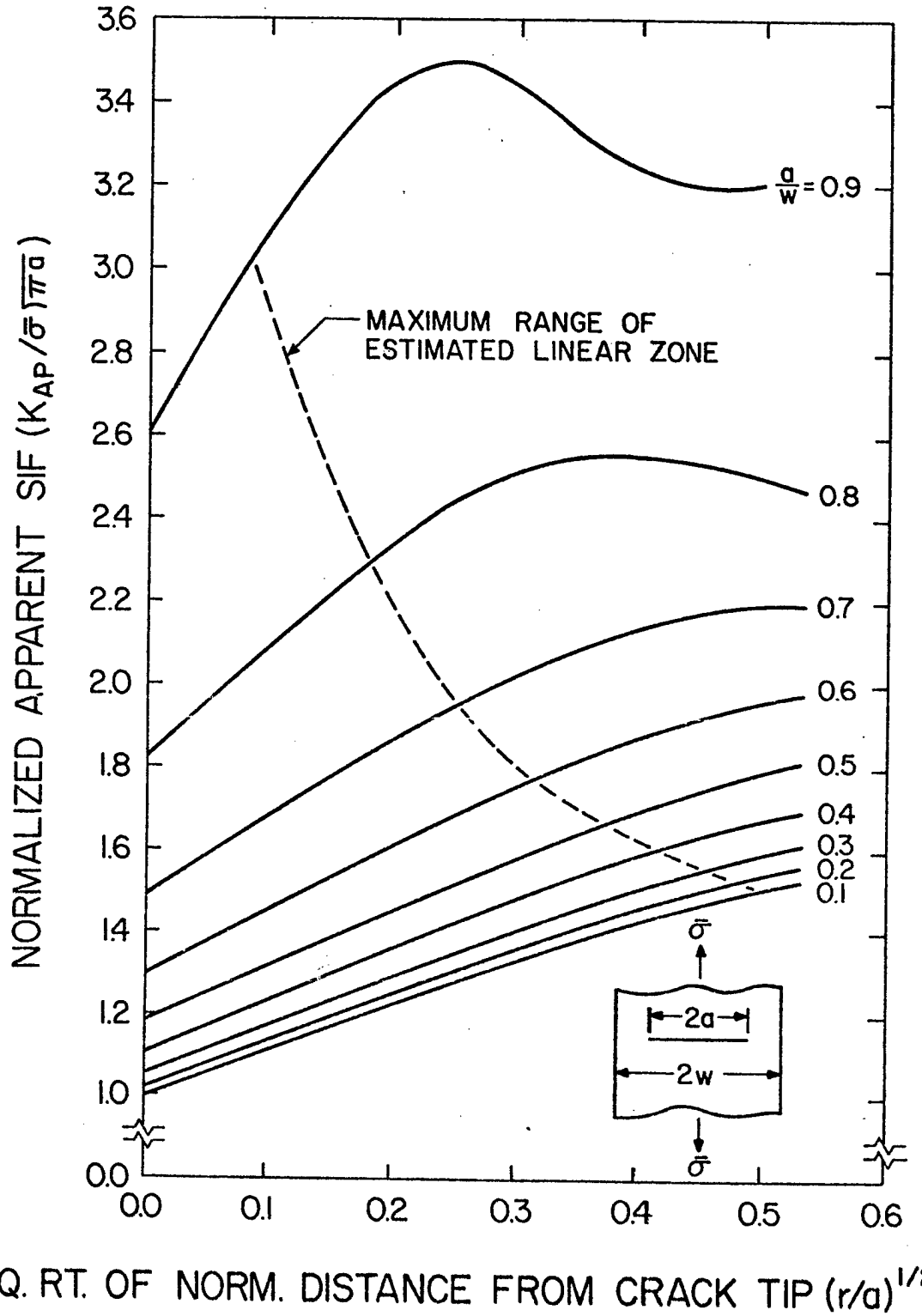

Figure 11. Normalized K_{AP} Curve for Through Crack in Finite Width Strip.

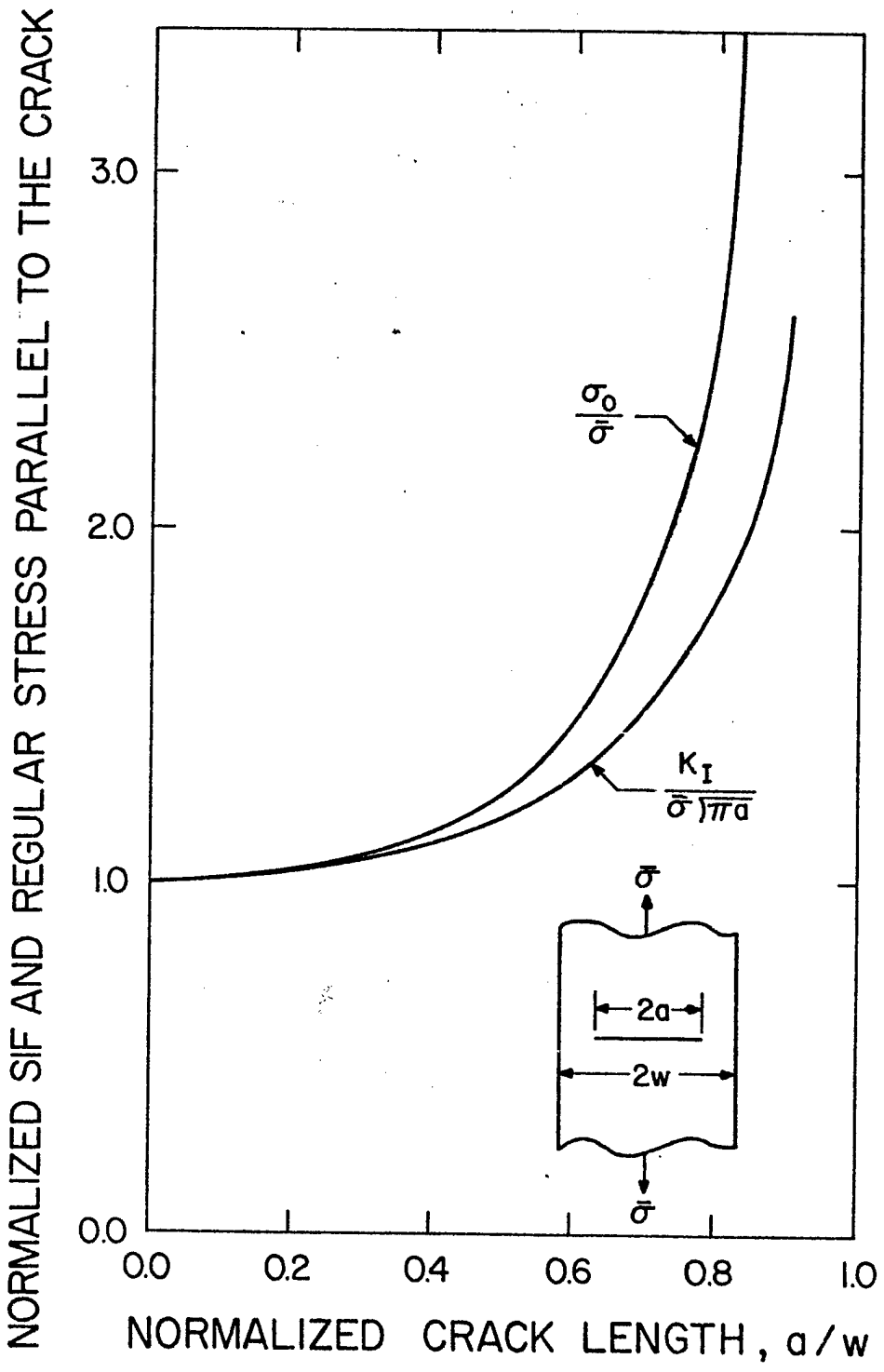

Figure 12. Normalized σ_0 and K_I Curves for Through Crack in Finite Width Strip.

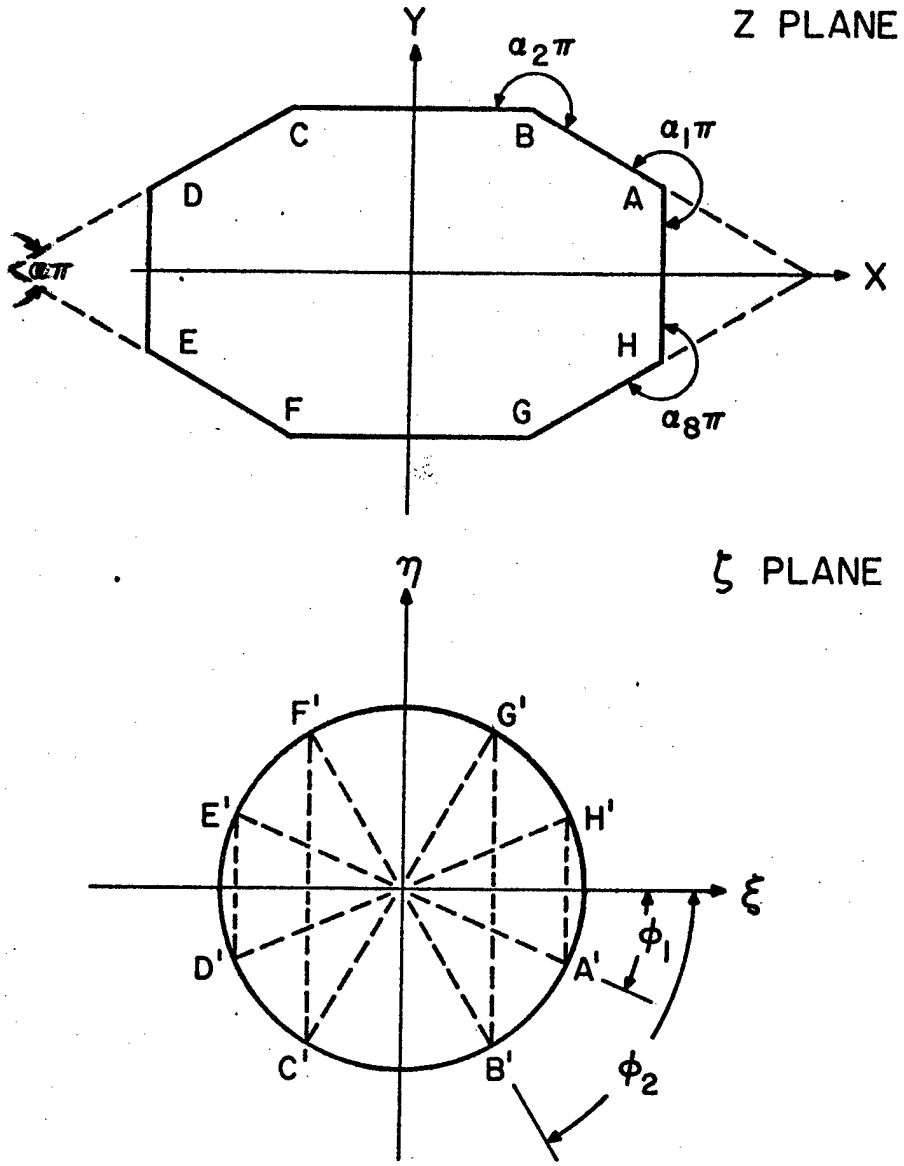

Figure A-1. Hole Geometry and Mapped Region for Notch Solutions.

DISTRIBUTION LIST

FOR THEMIS REPORTS

(Virginia Polytechnic Institute and State University)

Commanding General
U.S. Army Natick Laboratories
ATTN: Mr. E. W. Ross, Jr.
Natick, Mass. 01762

Lehigh University
ATTN: Dr. G. C. Sih
Bethlehem, Pa. 18015

Commanding Officer
Frankford Arsenal
ATTN: Mr. P. D. Flynn
Bridge & Tacony Streets
Philadelphia, Pa. 19137

Battelle Memorial Institute
ATTN: Dr. G. T. Hahn
505 King Avenue
Columbus, Ohio 43201

General Electric Company
ATTN: A. J. Brothers, Materials and Processes Lab.
Schenectady, New York 12010

United States Steel Corporation
ATTN: Mr. S. T. Rolfe, Applied Research Lab.
Monroeville, Pa. 15146

University of Illinois
ATTN: Mr. H. T. Corten, Department of Theoretical & Applied Mechanics
212 Talbot Lab.
Urbana, Illinois 61803

Westinghouse Electric Company
ATTN: Mr. E. T. Wessel, R&D Center
Pittsburgh, Pa. 15200

Carnegie Institute of Technology
ATTN: Dr. J. L. Swedlow
Schenley Park
Pittsburgh, Pa. 15213

Rensselaer Polytechnic Institute
ATTN: Prof. J. C. Janz, Chairman of Chemistry Department
Troy, New York 12180

Syracuse University
ATTN: Dr. H. W. Liu
Syracuse, New York 13210

Commanding Officer
U.S. Army Aviation Material Laboratories
ATTN: Mr. C. D. Roach
Fort Eustis, Virginia 23604

University of California
ATTN: W. W. Gerberich, Department of Mineral Technology
Berkeley, Calif. 94700

University of Illinois
ATTN: Prof. D. Drucker, Dean of School of Engineering
Champaign, Illinois 61820

University of Washington
ATTN: Prof. A. Kobayashi, Department of Mechanical Engineering
Seattle, Washington 98105

Technical Director
U.S. Army Materials & Mechanics Research Center
ATTN: Mr. J. Bluhm
Watertown, Mass. 02172

Brown University
ATTN: Dr. J. R. Rice
Providence, Rhode Island 02912

University of Connecticut
ATTN: Dr. A. J. McEvily, Head, Dept. of Metallurgy U-139
Dr. N. D. Greene, Metallurgy Dept.
Storrs, Conn. 06268

	Copies
Commandant HQ, U.S. Army Aviation School ATTN: Office of the Librarian Fort Rucker, Alabama 36362	1
Commanding Officer Frankford Arsenal Philadelphia, Pa. 19137	1
Commanding Officer Picatinny Arsenal Dover, New Jersey 07801	1
Commanding General Redstone Arsenal ATTN: Documentation & Technical Information Branch	2
AMSMI-RRS	1
AMSMI-RKK	1
AMSMI-RSM Alabama 35809	1
Commanding Officer Plastics Technical Evaluation Center ATTN: SMUPA-VP3 Picatinny Arsenal Dover, New Jersey 07801	1
Commanding Officer Watervliet Arsenal ATTN: SWEWV-RD Dr. R. E. Weigle	1
SWEWV-RDR Dr. I. Ahmad	1
SWEWV-RDR Dr. M. Hussain	1
SWEWV-RDR Dr. F. Saegusa	1
SWEWV-RDR Dr. J. H. Underwood	1
SWEWV-RDR Mr. J. F. Throop	1
SWEWV-RDR Mr. T. Pichily	1
SWEWV-RDR Mr. T. MacLaughlin	1
SWEWV-RDD Dr. V. J. Colangelo Watervliet, New York 12189	1
Mr. George Vrooman SWEWV-RDT-6 Document Libraries Watervliet Arsenal Watervliet, New York 12189	1
Mr. Charles Eldridge Structures and Mechanics Laboratory Research and Development Director U. S. Army Missile Command Huntsville, Alabama	1
Commanding Officer Watervliet Arsenal ATTN: SWEWV-RDT-TP, Mr. John Barnewall Watervliet, New York 12189	6

SECURITY CLASSIFICATION OF THIS PAGE *(When Data Entered)*

REPORT DOCUMENTATION PAGE

READ INSTRUCTIONS BEFORE COMPLETING FORM

1. REPORT NUMBER: VPI-E-74-13	2. GOVT ACCESSION NO.
3. RECIPIENT'S CATALOG NUMBER	
4. TITLE *(and Subtitle)*: A Study of Linear Very Near and Far Field Effects in Photoelastic Stress Intensity Determination	5. TYPE OF REPORT & PERIOD COVERED: Winter and Spring 1974
	6. PERFORMING ORG. REPORT NUMBER: VPI-E-74-13
7. AUTHOR(s): M. A. Schroedl and C. W. Smith	8. CONTRACT OR GRANT NUMBER(s): DAA-F07-69-C-0444
9. PERFORMING ORGANIZATION NAME AND ADDRESS: Dept. of Engr. Science & Mechanics, Virginia Polytechnic Inst. & State University, Blacksburg, Va. 24061	10. PROGRAM ELEMENT, PROJECT, TASK AREA & WORK UNIT NUMBERS: N. A.
11. CONTROLLING OFFICE NAME AND ADDRESS: Army Research Office, Office Chief Res. & Dev., ATTN: Col. Richard Ballard, 3045 Columbia Pike, Arlington, Va. 22207	12. REPORT DATE: July 1974
	13. NUMBER OF PAGES
14. MONITORING AGENCY NAME & ADDRESS *(if different from Controlling Office)*: Commanding Officer, Watervliet Arsenal, Watervliet, N. Y. 12198, ATTN: R. E. Weigle, Chief Scientist	15. SECURITY CLASS. *(of this report)*: N. A.
	15a. DECLASSIFICATION/DOWNGRADING SCHEDULE: N. A.

16. DISTRIBUTION STATEMENT *(of this Report)*

Approved for Public Release, Distribution Unlimited

17. DISTRIBUTION STATEMENT *(of the abstract entered in Block 20, if different from Report)*

Same as Item 16

18. SUPPLEMENTARY NOTES

Fracture Mechanics, Local stresses near cracks, Stress Intensity Factors

19. KEY WORDS *(Continue on reverse side if necessary and identify by block number)*

20. ABSTRACT *(Continue on reverse side if necessary and identify by block number)*

A technique known as the Taylor Series Correction Method (TSCM) for extracting the stress intensity factor from photoelastic data is reviewed. The need for "artificial" flaws is identified and an approach due to Savin is used to evaluate the near field effects of various practical artificial flaw shapes upon the apparent stress intensity factor. Using the Sneddon-Srivastav solution for a line crack in a finite width plate, the constriction of the singular zone is demonstrated as the crack tip approaches the free edge.

DD FORM 1 JAN 73 1473 EDITION OF 1 NOV 65 IS OBSOLETE

N.A.

SECURITY CLASSIFICATION OF THIS PAGE *(When Data Entered)*